Transcranial stimulation of alpha oscillations up-regulates the default mode network

It is widely recognized that the brain self-organizes into large-scale intrinsic networks. Such intrinsic organization is so fundamental to normal neural functioning that it commands 60 to 80% of the brain's energy (1). Two main mechanisms—intrinsic interregional connectivity and interneuronal synchrony—are thought to underpin the brain's organization (2–6). The default mode network (DMN), emerging from intrinsic interregional connectivity crisscrossing a large extent of the brain, occupies the apex of intrinsic connectivity networks (7) and dominates the brain's intrinsic activity (1, 8). Accordingly, the DMN supports advanced human mental faculties (e.g., consciousness, self-reference, social inference, remembering the past, and expecting the future) (8), while its dysregulation is characteristic of major neuropsychiatric disorders (e.g., DMN hyperconnectivity in major depression and hypoconnectivity in Alzheimer's disease, schizophrenia, and posttraumatic stress disorder) (9–12). However, mechanisms regulating the DMN remain elusive, while effective interventions for DMN dysregulation are lacking.

Interneuronal synchrony is thought to be inherently related to interregional connectivity and potentially bind and sculpt such connectivity through neural development (2–6). Importantly, the alpha (8 to 12 Hz) oscillation, the primary rhythm of intrinsic neural synchrony (13, 14), has been linked to the DMN functioning (4, 15). In fact, rapid advances in neuroimaging and neurocomputing have brought forward mounting evidence of multifaceted physiological and functional associations between the alpha oscillation and the DMN. Physiologically, resting-state (RS) simultaneous EEG-fMRI (electroencephalography and functional MRI) recordings have revealed intrinsic positive coupling between alpha oscillations and DMN activity (16–20). Of particular relevance, akin to its role in long-range neural communication, alpha oscillations are found to be the primary neural synchrony linking the posterior and anterior hubs of the DMN (the posterior cingulate cortex [PCC] and medial prefrontal cortex [mPFC], respectively) (15, 19, 21, 22). Functionally, alpha oscillations and the DMN are both involved in disengaging the brain from the sensory environment and maintaining the RS (1, 13, 23), while alpha desynchrony and DMN dysconnectivity, including specific disruption of alpha-oscillatory PCC-mPFC connectivity, co-occur in several major neuropsychiatric disorders (e.g., Alzheimer's disease, schizophrenia, and posttraumatic stress disorder) (24–26).

Nonetheless, these associations between alpha oscillations and the DMN remain correlational in nature, calling for experimental investigation to ascertain their mechanistic linkage. Owing to the proximity of its primary source (the occipitoparietal cortex) to the scalp, the alpha oscillation is highly responsive to transcranial stimulation (27–30) and can be a viable target for experimental manipulation. Among the many transcranial stimulation technologies, transcranial alternating current stimulation (tACS) applies frequency-specific sinusoidal electric currents through the scalp, which is uniquely advantageous in mimicking and entraining endogenous oscillations by tuning

Author contributions: K.J.C. and W.L. designed research; K.J.C., J.A.A., Y.Y., and W.L. performed research; J.T.R. and M.D. contributed new reagents/analytic tools; K.J.C., J.A.A., J.T.R., M.D., and W.L. analyzed data; and K.J.C., J.A.A., M.D., and W.L. wrote the paper.

The authors declare no competing interest.

This article is a PNAS Direct Submission.

[1]To whom correspondence may be addressed. Email: clancy@psy.fsu.edu or wenli@psy.fsu.edu.

NEUROSCIENCE

PSYCHOLOGICAL AND COGNITIVE SCIENCES

not only the frequency and amplitude but also the oscillatory phase. The latter, by enhancing phase synchronization, could be particularly effective at facilitating interregional connectivity (31). Therefore, we experimentally manipulated alpha oscillations with MR-compatible high-definition (HD) alpha-frequency tACS (α-tACS) targeting the occipitoparietal alpha source. Using RS simultaneous EEG-fMRI recordings, we measured concurrent changes in alpha synchrony (EEG alpha power and connectivity) and DMN connectivity (fMRI blood oxygen level–dependent [BOLD] connectivity) before and after tACS (versus Sham control) and tested the hypothesis that enhanced alpha synchrony via tACS can facilitate the synchronization of BOLD fluctuations, resulting in increased DMN connectivity.

Results

Validation of tACS Efficacy (α-tACS Increased Alpha Power and Connectivity). We applied HD tACS using a 4 × 1 montage over midline occipitoparietal sites (with 4 surrounding + 1 central electrodes forming a closed circuit; Fig. 1A), which were selected to maximally target the primary alpha cortical source—the occipitoparietal cortex (13, 14, 28). Previous work has demonstrated the efficacy and reproducibility of this tACS protocol in augmenting both alpha local power and long-range connectivity (28). Finite-element model simulation of the current distribution based on a standard head model confirmed

maximal electric fields (0.21 V/m) in the occipitoparietal cortex (peaking at the occipito–parietal junction; x, y, z = 16, −86, 36), relative to minimal electric fields (< 0.02 V/m) in frontal regions. Another finite-element model estimation based on a realistic head model (the average T1 of the Active group) yielded a similar distribution of the current (*SI Appendix*, Fig. S1). Source-level analysis of EEG alpha power in the Active group showed maximal alpha power increase in the right occipitoparietal cortex (Fig. 1B). In sum, these results confirmed that our tACS accurately targeted the occipitoparietal cortex.

Importantly, in support of the efficacy of α-tACS, we observed increases in right posterior alpha power and right posterior-to-frontal (P→F) alpha connectivity in the Active (versus Sham) group from pre- to poststimulation (Fig. 1 C–G). These effects, including the right-hemisphere dominance, replicated our previous tACS findings (28). Specifically, after tACS, the Active group ($n = 17$) showed significant increase in right posterior alpha power from the baseline ($t = 2.69$, $P = 0.015$), while no change was observed in the Sham group ($n = 19$; $P = 0.92$; Fig. 1 C–E). A double contrast (Post − Pre$_{Active − Sham}$) further confirmed specific alpha power increase in the Active (versus Sham) group ($t = 2.14$, $P = 0.040$). Left posterior alpha power also increased in the Active group ($t = 2.16$, $P = 0.045$), which, however, failed to survive the double contrast ($t = 1.36$, $P = 0.184$). As evinced by recent neural computational and electrophysiological (including intracranial recordings) studies,
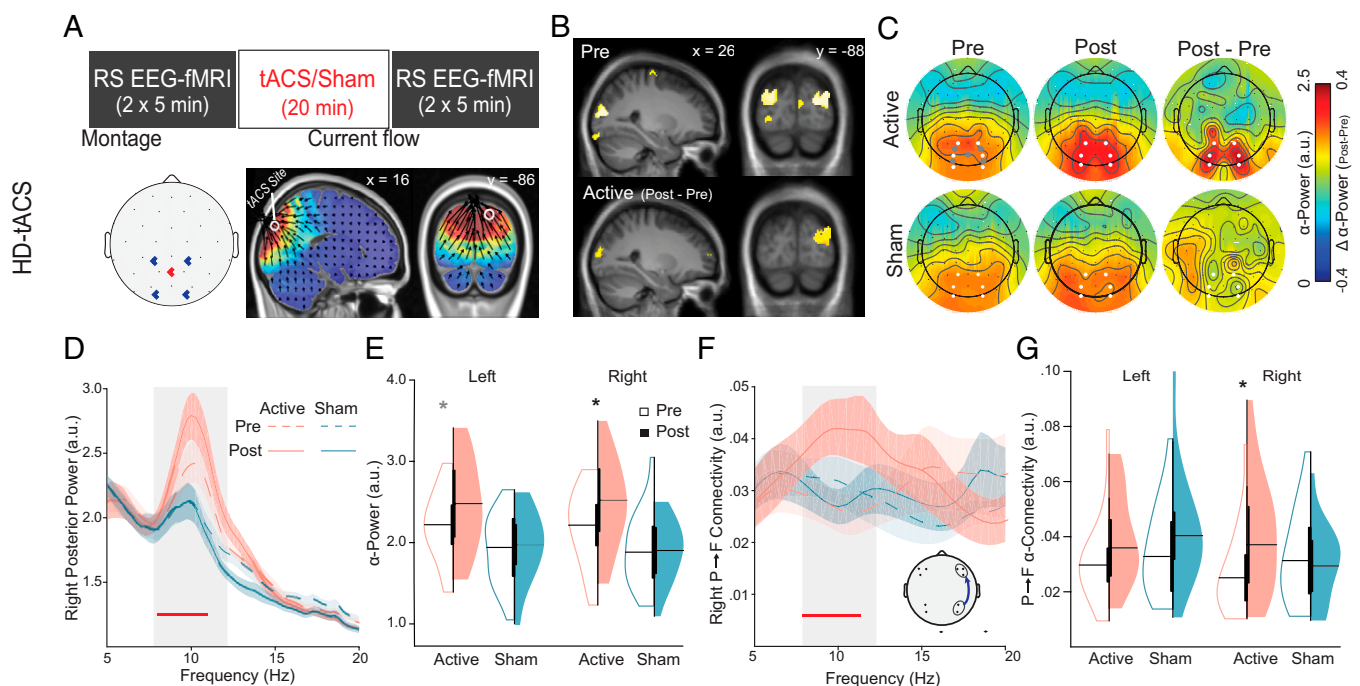

Fig. 1. α-tACS protocol and efficacy validation. (*A*) Experimental design. Participants underwent RS EEG-fMRI recordings immediately before and after tACS/Sham stimulation. HD tACS was administered over the occipitoparietal midline with a 4 × 1 montage (4 surrounding + 1 central electrodes forming a closed circuit). Finite-element modeling of the current flow based on a standard head model indicated maximal and focal electric fields (0.21 V/m) in the occipitoparietal cortex (peaking at the occipito–parietal junction, as indicated by the white circle; x, y, z = 16, −86, 36; Montreal Neurological Institute coordinates), relative to minimal electric fields (<0.02 V/m) in frontal regions. (*B*) We further localized the source of alpha power to the bilateral occipito-parietal cortex (display threshold (*P* < 0.001 familywise error rate, k = 20; *Top*). Source-level alpha power increase after tACS was further localized to the right occipitoparietal cortex (display threshold *P* < 0.05, k = 10; *Bottom*). (*C*) Topography of alpha (8 to 12 Hz) power before and after stimulation. Gray dots in the *Top Left* indicate tACS montage. White dots indicate left and right occipitoparietal electrodes from which alpha power was extracted. (*D*) Spectral waveforms averaged across the right occipitoparietal electrodes demonstrate specific increases in the Active (versus Sham) group, which were restricted to the alpha frequency (gray box); the red bar indicates frequency bins (0.25 Hz each) showing significant tACS effects; Ribbon = SEM. (*E*) Violin plots for alpha power over left and right electrodes indicate significant right posterior power increase in the Active group. (*F*) Right-hemisphere P→F GC waveforms demonstrate specific increases in the Active (versus Sham) group, which were restricted to the alpha frequency (gray box); the red bar indicates frequency bins (0.5 Hz each) showing significant tACS effects; *Inset* shows ipsilateral electrode pairs used for alpha GC as used in our prior studies (28, 63, 64); Ribbon = SEM. (*G*) Violin plots for alpha-frequency P→F GC in the left and right hemispheres indicate significant right-hemispheric GC increase in the Active group. *P < 0.05 (black/gray: surviving double/single contrast).

Clancy et al.
Transcranial stimulation of alpha oscillations up-regulates the default mode network

alpha projections track a selective P→F direction (i.e., directed alpha P→F connectivity) via P→F cortical synchronization or traveling waves (15, 21, 22, 32–36). We thus used Granger causality (GC) analysis to examine changes in this alpha connectivity. We found that the Active group also exhibited an increase in right-hemispheric alpha P→F connectivity ($t = 2.36$, $P = 0.031$), which was again absent in the Sham group ($P = 0.621$; Fig. 1 F and G and *SI Appendix*, Fig. S3). A similar double contrast confirmed that this alpha connectivity increase was specific to the Active group ($t = 2.12$, $P = 0.042$). Exploratory analyses of opposite F→P connectivity showed no effect of tACS (*SI Appendix*). Finally, as illustrated in Fig. 1 D and F, both power and connectivity increases were constrained to the alpha frequency, highlighting the specific tACS effects on alpha oscillations.

α-tACS Increased DMN BOLD Connectivity. Extracting RS fMRI BOLD timeseries from the DMN regions of interest (ROIs)—midline hubs (mPFC and the ventral and dorsal subdivisions of PCC—vPCC and dPCC) and a key lateral node (left/right angular gyrus [ANG])—before and after stimulation, we conducted ROI-based functional connectivity analysis (followed by multiple comparison correction based on the false discovery rate [FDR]). The Active group demonstrated increases in vPCC-mPFC ($t = 2.87$, $P = 0.011$) and vPCC-rANG ($t = 3.12$, $P = 0.007$) connectivity after tACS (Fig. 2 A–C). There was no change in the Sham group (p's > 0.13), while double contrasts (Post - Pre$_{Active - Sham}$) further confirmed these increases were specific to the Active group (t's > 2.79, p's < 0.009, FDR P < 0.05). Whole-brain vPCC-seed connectivity maps (of both simple and double contrasts) confirmed these results and, importantly, indicated that the increases were largely constrained to the DMN (Fig. 2C and *SI Appendix*, Fig. S2).

α-tACS Increased DMN Alpha-Frequency Connectivity. We then examined the effect of tACS on source-level (DMN) alpha P→F connectivity. A double contrast (Post − Pre$_{Active - Sham}$) showed a specific increase in alpha PCC→mPFC connectivity in the Active (versus Sham) group ($t = 2.27$, $P = 0.030$; Fig. 2 D–F) after stimulation. Specifically, the Active group showed an increase ($t = 1.74$, $P = 0.049$, one-tailed), while the Sham group trended toward a decrease ($t = −1.48$, $P = 0.079$, one-tailed) in this connectivity. The alpha rANG→mPFC connectivity was not affected by tACS ($P = 0.92$). Exploratory analyses of alpha horizontal connectivity between rANG and PCC (in both directions) and opposite F→P alpha connectivity (i.e., mPFC→PCC and mPFC→rANG) showed no effect of tACS (p's > 0.440). Finally, in keeping with these ROI-based results, whole-brain maps of causal connectivity (GC) from the PCC indicated specific increase (in the Active versus Sham group) from the PCC to the mPFC, including the mPFC ROI and the rostral anterior cingulate cortex/ACC (Fig. 2E).

Alpha Increase Mediated DMN Connectivity Enhancement via α-tACS. Correlational analysis showed that increases in BOLD vPCC-mPFC connectivity from the baseline strongly correlated with increases in alpha P→F connectivity ($r = 0.59$, $P < 0.001$; Fig. 3A; given the significant enhancement of right-hemisphere GC by tACS, we correlated this right lateral GC change with DMN connectivity change). Furthermore, this correlation was significant within the two groups individually (Active: $r = 0.51$, $P = 0.030$; Sham: $r = 0.49$, $P = 0.047$), highlighting the robust, inherent coupling between DMN and alpha connectivity. Changes in P→F connectivity in other (delta, theta, and beta) frequencies showed no such association (p's > 0.111), demonstrating a unique association between changes in alpha-frequency connectivity and DMN connectivity. Furthermore, increases in BOLD vPCC-rANG did not correlate with alpha

connectivity ($r = 0.14$, $P = 0.545$), highlighting the association of alpha P→F connectivity with DMN posterior–anterior connectivity. Importantly, a mediation analysis of tACS modulation of BOLD vPCC-mPFC connectivity revealed a significant indirect effect of alpha P→F connectivity (beta = 0.076, CI = [0.018 0.189]), suggesting that increases in alpha P→F connectivity mediated the effect of tACS on BOLD vPCC-mPFC connectivity (Fig. 3B).

α-tACS Increased Connectivity between the tACS Site and the DMN. To attain mechanistic insights into tACS-induced neuromodulation, we examined BOLD connectivity between the tACS site (a 10-mm sphere around the voxel with maximal electrical field of tACS; Fig. 1A) and the DMN. Active group demonstrated vPCC–tACS$_{site}$ (site of tACS) connectivity increase after tACS ($t = 3.73$, $P = 0.002$), while the Sham group showed no change ($P = 0.578$; Fig. 4A). A double contrast further confirmed the specific increase in the Active (versus Sham) group ($t = 2.30$, $P = 0.028$). The Active group showed tACS$_{site}$-mPFC connectivity increase after tACS ($t = 2.89$, $P = 0.011$), while the Sham group showed no change ($P = 0.836$). Again, a double contrast confirmed that the increase was specific to the Active (versus Sham) group ($t = 1.75$, $P = 0.045$ one-tailed). No effects of tACS emerged in the tACS$_{site}$-rANG connectivity (p's > 0.272). Whole-brain tACS$_{site}$ seed-based connectivity analysis confirmed these results while showing little connectivity change outside the DMN (*SI Appendix* and Fig. 4B).

Replication and Control Study (HD EEG-tACS). To further specify α-tACS effects and exclude frequency-independent effects of electrical stimulation, we conducted an independent α-tACS study ($n = 34$) with an active control condition (transcranial random noise stimulation [tRNS]). We found significant increases in right posterior alpha power ($t = 3.72$, $P = 0.00073$) and right-hemisphere P→F alpha connectivity ($t = 2.09$, $P = 0.044$) following α-tACS but not tRNS (p's > 0.217). Similarly, at the source level, we observed significant increase in alpha-frequency DMN (PCC→mPFC) connectivity ($t = 2.28$, $P = 0.029$) after α-tACS but not tRNS ($P = 0.246$). Together, these results not only replicated the findings in the main study but also highlighted the specific α-tACS effects. More study details are provided in *SI Appendix*.

Discussion

Combining MR-compatible HD α-tACS with simultaneous EEG-fMRI, we demonstrated that α-tACS of the alpha source in the occipitoparietal cortex not only augmented alpha oscillations but also strengthened BOLD and alpha-frequency oscillatory connectivity within the DMN. Importantly, tACS-induced augmentation of P→F alpha connectivity mediated the tACS enhancement of BOLD connectivity between DMN hubs (vPCC-mPFC). By contrast, no tACS effects emerged outside the alpha frequency or the DMN. These findings thus indicate that the DMN can be up-regulated by transcranial stimulation of alpha oscillations. Moreover, they provide experimental evidence to mechanistically link alpha oscillations, particularly alpha connectivity, to the DMN, lending further credence to the notion of alpha-DMN interdependence (4, 15).

Posterior alpha power and P→F alpha connectivity reflect local alpha synchrony in the occipitoparietal cortex and long-range synchrony from the occipitoparietal cortex to the frontal cortex, respectively. Our EEG data confirmed that tACS enhanced alpha power in the targeted occipitoparietal cortex as well as P→F connectivity, suggesting tACS modulation of both local and distant interareal synchrony. While these two types of tACS modulation often co-occur, they can be dissociated. For instance, our previous tACS study demonstrated that enhanced P→F alpha connectivity persisted 24 h after tACS even though
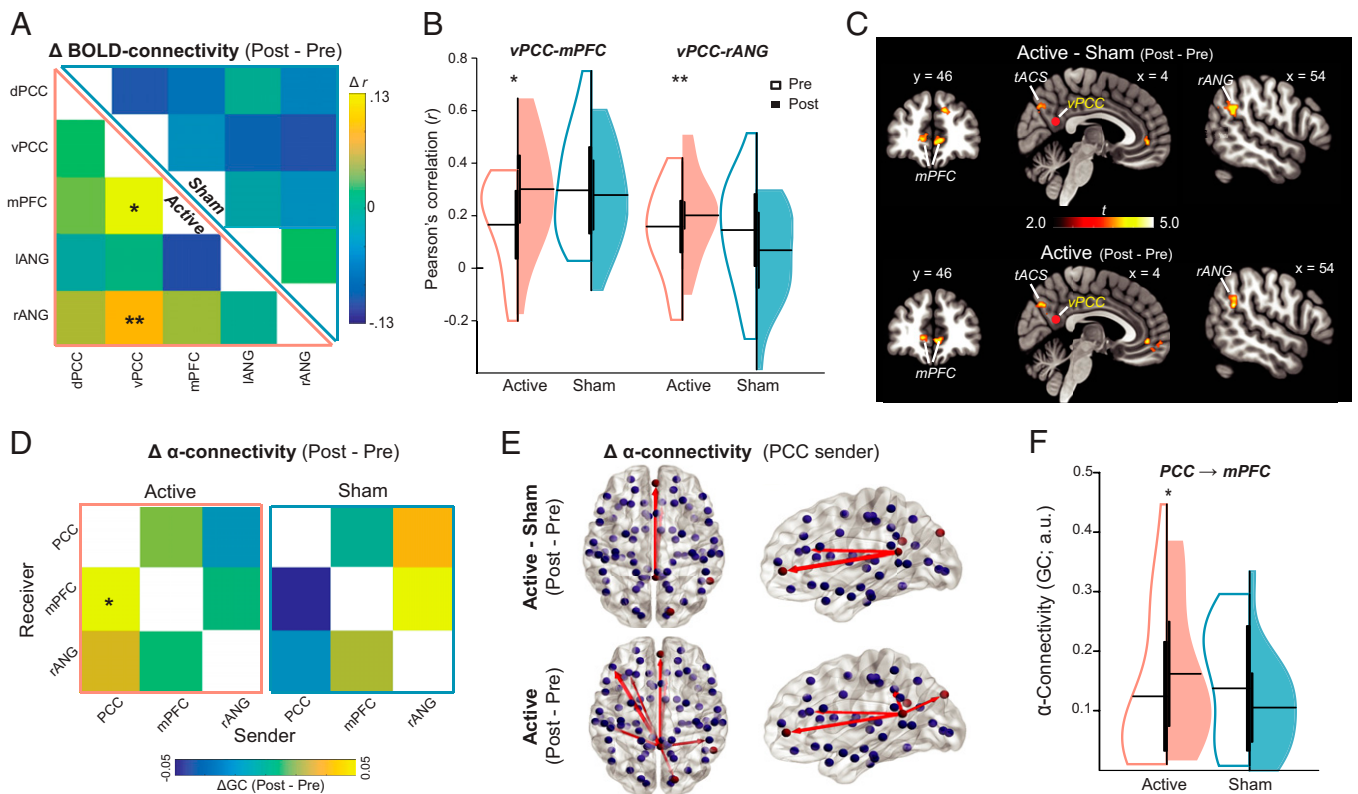
Clancy et al.
Transcranial stimulation of alpha oscillations up-regulates the default mode network

PNAS | 3 of 8
https://doi.org/10.1073/pnas.2110868119

Fig. 2. α-tACS enhanced BOLD and alpha connectivity in the DMN (hypothesis testing). (*A*) Post- versus prestimulation connectivity matrix for the Active (*Lower* half) and Sham Control (*Upper* half) groups and (*B*) their respective violin plots demonstrate that tACS increased DMN connectivity (vPCC-mPFC and vPCC-rANG). (*C*) vPCC-seed whole-brain connectivity maps further indicate that increases in vPCC connectivity (in both the double and single contrasts) were largely restricted to the DMN (bilateral mPFC, rANG) and the tACS site (display threshold at $P < 0.005$ uncorrected, $k > 10$). (*D*) The Active group further demonstrated increases in alpha-frequency PCC→mPFC (GC), which also survived the double contrast (versus changes in the Sham group). Given the low spatial resolution of source-level EEG analysis, we combined ventral and dPCC into a single ROI of PCC. (*E*) Whole-brain maps of tACS enhancement of α-connectivity from the PCC. Paths depicted (PCC→mPFC and PCC→rostral ACC) survived both the double (*Top*) and single (*Bottom*) contrasts ($P < 0.05$, one-tailed; line thickness indicates strength of connectivity increase). Nodes represent whole-brain Brodmann Areas (blue color) and a priori DMN ROIs (red color). (*F*) ROI-based PCC→mPFC violin plot. *$P < 0.05$, **$P < 0.01$ (black/gray: surviving double/single contrast); black/solid line = double contrast, gray/dotted line = single contrast. Red dot indicates vPCC seed.

alpha power had returned to the baseline (28). By potentially strengthening oscillatory circuits via spike timing–dependent plasticity and long-term potentiation at the synapse (37, 38), α-tACS can exert (immediate and lasting) effects on long-range neural communication (i.e., alpha-frequency connectivity) (28, 30) and BOLD connectivity (39–41) beyond local power enhancement (via neural entrainment).

However, network-level effects have been examined in only a handful of α-tACS-fMRI studies, which, using varied stimulation montages and protocols, have yielded ambiguous findings (39–41). Capitalizing on the selective P→F projection of alpha oscillations (15, 21, 22, 32–36), we applied HD tACS for concentrated stimulation of alpha generators in the occipitoparietal cortex (42) to optimize network-level modulation. Intracranial current flow estimation (based on both a standard and a realistic head model) confirmed focal electrical fields in the targeted region. In consequence, not only did tACS enhance alpha P→F connectivity, but our mediation analysis also showed that this tACS enhancement of alpha P→F connectivity contributed to tACS up-regulation of DMN connectivity.

tACS did not affect horizontal or F→P alpha connectivity on either surface or source level (*SI Appendix*), suggesting that tACS primarily serves to amplify the underlying endogenous activity (i.e., P→F alpha projection). Relatedly, despite the midline montage, the effects of α-tACS on alpha posterior power and P→F connectivity emerged in the right hemisphere

primarily, consistent with our previous α-tACS study using the same tACS parameters (28). Given the right-hemisphere dominance of alpha oscillations in various basic processes (43), we suspect that this hemispheric asymmetry of tACS effects is also aligned with the underlying alpha functioning. Control analyses also explored potential tACS effects outside the alpha frequency and the DMN. Analyses across the frequency spectrum (1 to 30 Hz) ascertained that the tACS effects were specific to the alpha frequency (*SI Appendix*). Similarly, whole-brain connectivity analysis seeded in the PCC or the tACS site further confirmed increased connectivity within the DMN and not outside the DMN (even at a lenient threshold of $P < 0.01$ uncorrected). These results highlight the critical contribution of alpha oscillations to the integrity of the DMN.

Increased BOLD connectivity between the tACS site and DMN hubs (PCC and mPFC; *SI Appendix*) suggest that superficial transcranial stimulation can reach the two hubs of the DMN via the tACS site and synchronize their activity, thereby inducing the up-regulation of the network. It is worth noting that the mPFC, a deep and distal structure that is critically implicated in emotional disorders, is often difficult to access via noninvasive stimulation (44). Our findings thus have important clinical implications by identifying a viable pathway for noninvasive intervention to modulate this pivotal structure.

Purportedly, given the prominent role of the PCC in the DMN, tACS modulation of the PCC could result in particularly
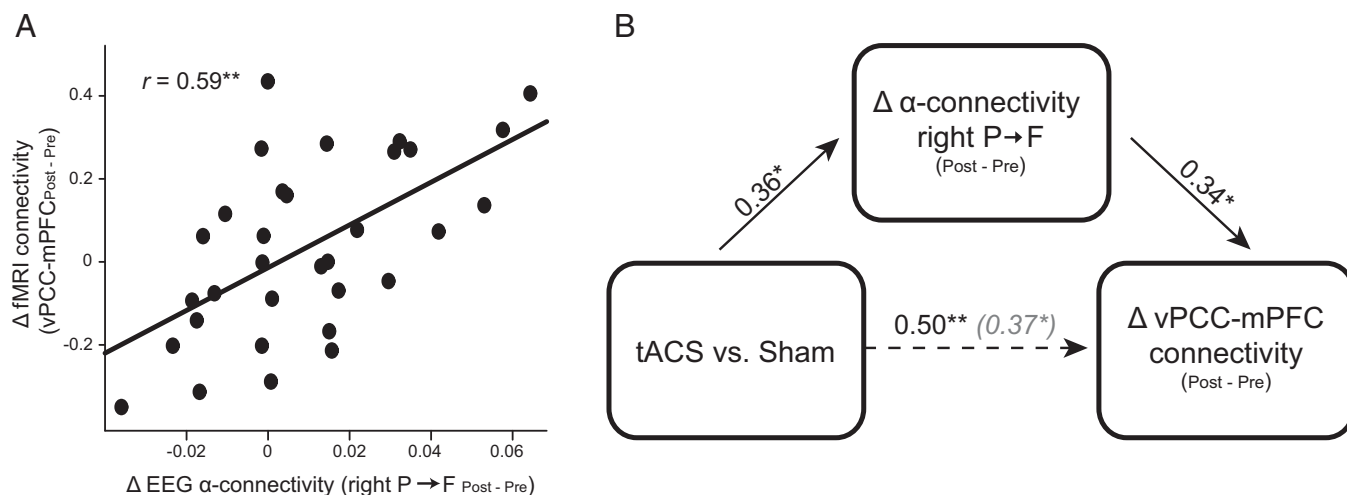
Fig. 3. Alpha P→F connectivity increase mediated DMN connectivity enhancement via α-tACS. (*A*) Scatterplot demonstrating a positive correlation between changes in BOLD vPCC-mPFC connectivity and right-hemisphere P→F alpha-frequency connectivity/GC. (*B*) Mediation model demonstrating indirect (i.e., mediation) effect of tACS group on increases in DMN connectivity through increases in right-hemisphere P→F alpha-frequency GC. Path strengths are indicated by standardized beta coefficients. The parenthetical beta coefficient reflects the direct path strength after controlling for changes in P→F GC. *$P < 0.05$, **$P < 0.005$.

salient DMN effects (i.e., BOLD vPCC-mPFC and alpha PCC→mPFC connectivity). Furthermore, the impact of α-tACS also reached the lateral connection between the vPCC and the rANG, suggesting that enhanced connectivity of DMN midline core would propagate to the rest of the network. This finding could highlight the robust self-organization of an intrinsic connectivity network, enabling network-wide modulation. The anatomy of the DMN has been increasingly refined since its initial characterization. Within the midline core, there are actually two interdigitated subnetworks, in which the PCC hub is divided into a vPCC and a dPCC, with the former connected with the mPFC hub (the anterior and ventral mPFC) and the latter with the dorsal mPFC (8, 45, 46). Accordingly, the vPCC is thought to be a primary hub for the DMN, relative to the dPCC that is likely a connector hub between the DMN and other networks (e.g., the salience network, the visual network) (46). In keeping with that, our separate examination of the ventral and dorsal subdivisions of the PCC (i.e., vPCC and dPCC) isolated tACS effects on vPCC- but not dPCC-related DMN connectivity. In fact, exploratory analysis of dPCC-seeded whole-brain connectivity revealed no clear effects of tACS

($P < 0.01$ uncorrected; *SI Appendix*, Fig. S2). These findings further accentuate the close association between alpha oscillations and the core of the DMN.

While mounting evidence indicates the physiological coupling and functional similarity between alpha oscillations and the DMN, they have been correlational in nature (1, 13, 16–20, 23, 24, 26). Our experimental manipulation of alpha oscillations via tACS lends mechanistic support for the DMN–alpha association, reinforcing the hypothesis that the intrinsic connectivity networks have an electrophysiological origin (4) and, specifically, that alpha oscillations underpin the DMN (15). Yet to be revealed are the precise physiological processes that underlie this association. It is possible that neural synchrony via alpha oscillations directly synchronizes BOLD fluctuations across the DMN, thereby enhancing DMN connectivity. However, as indicated by the mediation analysis (Fig. 3*B*), the effect of tACS modulation on DMN connectivity enhancement remained significant after controlling for the contribution of alpha P→F connectivity, suggesting additional mechanisms were at play.

We surmise that the DMN and alpha oscillations, two primary architectures of the brain's organization, may be united
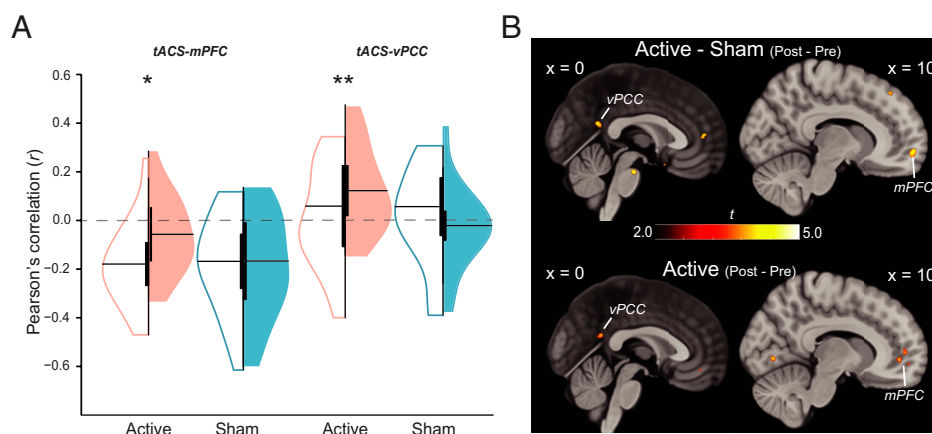

Fig. 4. Increased connectivity between tACS site and DMN. (*A*) Violin plots demonstrate that tACS increased connectivity between the tACS site and midline DMN hubs (tACS-mPFC and tACS-vPCC). (*B*) tACS$_{site}$ seed-based whole-brain connectivity maps further indicate increases in tACS connectivity to midline DMN hubs for the Active group alone ($P < 0.005$ uncorrected, $k > 10$). *$P < 0.05$, **$P < 0.01$.

Clancy et al.
Transcranial stimulation of alpha oscillations up-regulates the default mode network

PNAS | 5 of 8
https://doi.org/10.1073/pnas.2110868119

and synergized by a more fundamental organizational architecture—the thalamocortical circuitry (47). The thalamocortical circuitry is long known to generate, sustain, and regulate alpha oscillations (48, 49). Recently, the thalamocortical circuitry has been proposed to be a key controller of the DMN (8). Particularly, thalamocortical circuits (including the thalamus, sensory cortex, and thalamic reticular nucleus) that regulate alpha oscillations are also posited to regulate the DMN by inhibiting sensory feedforward projection, regulating wakefulness and arousal, and orchestrating large-scale brain activities (8). In line with this thalamocortical hypothesis, modulation of alpha oscillations can affect the thalamocortical circuitry, which then up-regulates the DMN. Future research into the interrelations between thalamocortical circuitry and the DMN, specifically through alpha activity, would further elucidate this mechanism.

That the thalamocortical circuitry could serve as the backbone of the brain's organizational architecture (47) and regulate both the DMN and alpha oscillations would account for the prevalent thalamocortical dysfunctions, in both connectivity (thalamocortical dysconnectivity) and neural synchrony (thalamocortical dysrhythmia), in major neuropsychiatric disorders (49–51). Accordingly, therapies effectively regulating this circuitry would bring forward major breakthroughs in neuropsychiatric treatment, and noninvasive neuromodulation of alpha oscillations could be a prime candidate for such interventions.

Materials and Methods

Participants. In total, 41 healthy volunteers (24 female, 20.8 ± 3.2 y of age) participated in the study after providing written, informed consent. This study was approved by the Florida State University Institutional Review Board. No participants reported a history of neurological or psychiatric disorders or current use of psychotropic medication. Participants were randomly assigned to two groups, an Active ($n = 21$) and a Sham group ($n = 20$). Two participants (Active $n = 2$) terminated their participation prematurely due to discomfort in the scanner. Three participants (Active $n = 2$, Sham $n = 1$) were excluded from fMRI analyses due to excessive motion (defined by > 5% of scans exceeding a framewise displacement index of 0.5 mm) (52), resulting in a final sample of 36 participants for fMRI analyses (Active $n = 17$, Sham $n = 19$). Four separate participants (Active $n = 1$, Sham $n = 3$) were excluded from EEG analyses due to significant artifacts, resulting in a final sample of 35 participants for EEG analyses (Active $n = 18$, Sham $n = 17$). Participants in the two groups did not differ in age or gender distribution (p's > 0.50).

Experimental Design. The experiment consisted of three phases: prestimulation RS recordings, tACS/Sham stimulation, and poststimulation RS recordings. In both pre- and poststimulation phases, participants underwent two successive 5-min simultaneous EEG-fMRI scans (with eyes open and fixated on a central crosshair). The MR-compatible stimulation was fully integrated with simultaneous EEG-fMRI recordings such that it did not require transition between the RS recording phases.

tACS. Alpha-frequency stimulation was administered with a ±2 mA sinusoidal current oscillating at 10 Hz using an MR-compatible HD tACS system (Soterix Medical, New York, NY). Stimulation electrodes were placed in a 4 × 1 montage over midline occipitoparietal sites (with 4 surrounding + 1 central electrodes forming a closed circuit; Fig. 1A), which were selected to maximally target the primary cortical source of alpha oscillations—occipitoparietal cortex (13, 14, 28).

α-tACS or Sham stimulation was administered for 20 min. To minimize awareness of experimental condition, the Sham group received α-tACS for 10 s at the beginning and the end of the phase. All participants completed a standard continuous performance task, which, by maintaining alertness, would enhance α-tACS efficacy (53). All participants were first told they would receive electrical stimulation and were informed of their true assignment during the debriefing at the end of experiment. Participants' blindness to the group assignment was confirmed via a funnel interview at the debriefing, which was further corroborated with the Adverse Effects Questionnaire at the end of experiment (54). Specifically, the Active and Sham groups showed no difference in their subjective experiences during the stimulation period ($t = 0.81$, $P = 0.423$) or the degree to which they attributed these sensations to the stimulation ($t = 1.23$, $P = 0.225$).

EEG Acquisition and Analyses. EEG data were recorded simultaneously with fMRI using a 64-channel MR-compatible EEG system (Brain Products GmbH, Germany). An additional electrode was placed on the participant's upper back to record electrocardiogram for cardioballistic artifact correction. The EEG recording system was synchronized with the fMRI scanner's internal clock throughout acquisition to facilitate successful removal of MR gradient artifact (16). Cardioballistic and gradient artifact corrections were performed offline using an average artifact template subtraction method as implemented in Brain Vision Analyzer 2.0 (Brain Products GmbH). Details regarding EEG artifact correction and additional preprocessing are provided in *SI Appendix*.

Power of alpha-frequency oscillations were computed using the multitaper spectral estimation technique. Directed alpha-frequency connectivity was assessed using GC analysis. Source-level analysis of alpha activity was performed using the Fieldtrip toolbox implemented in the Statistical Parametric Mapping Software, 12th Edition (SPM12) (55) , with the head model defined by each participant's T1 scan. To maintain the temporal resolution needed to compute GC, source-based alpha-frequency connectivity was assessed based on ROI timeseries derived from Exact Low-Resolution Electromagnetic Tomography (eLORETA) (56). Source-based GC analysis applied the same criteria as surface-level GC analysis. Additional details are provided in *SI Appendix*, Table S1 and Fig. S2.

MRI Acquisition and Preprocessing. Gradient-echo T2-weighted echoplanar images were acquired on a 3T Siemens Prisma MRI scanner using a 64-channel head coil with axial acquisition. Imaging parameters included TR/TE: 1,800/22.40 ms; slice thickness 1.8 mm; gap 0.45 mm; in-plane resolution/voxel size 1.8 × 1.8 mm; multiband acceleration factor = 2 (57); GeneRalized Autocalibrating Partial Parallel Acquisition (GRAPPA) acceleration factor = 2. A high-resolution (0.9 × 0.9 × 0.9 mm3) three-dimensional Magnetization Prepared Rapid Acquisition Gradient Echo (3D-MPRAGE) T1 scan was also acquired. Imaging data were preprocessed using SPM12, including slice-time correction, spatial realignment, and normalization using Diffeomorphic Anatomical Registration Through Exponentiated Lie algebra. To further remove artifacts potentially contributing to spurious RS activity variance (52), we implemented additional preprocessing using the Data Processing Assistant for Resting-State fMRI (DPARSFA) toolbox: 1) mean centering and whitening of timeseries; 2) temporal bandpass (0.01 to 0.08 Hz) filtering; 3) general linear modeling to partial out head motion with 24 nuisance variables (six head motion parameters each from the current and previous scan and their squared values); and 4) scrubbing of significant motion ("spikes") based on framewise displacement index (FDi > 0.5 mm). Further details are provided in *SI Appendix*.

ROIs. ROIs consisted of key nodes of the DMN, including the midline hubs, PCC and mPFC, and the bilateral ANG (58). Masks for the mPFC and ANG ROIs were drawn from the Willard Atlas (59). The PCC hub consists of functionally dissociable ventral and dorsal subdivisions, specifically the vPCC primarily linking DMN nodes and the dPCC with extensive extra-DMN connections (8, 46). We thus extracted masks for the vPCC and dPCC subdivisions individually from the Brainnetome Atlas (60). Since these masks were not applicable for low-resolution source EEG tomography (as in eLORETA), we applied 10-mm spheres around their respective coordinates established in the literature (26, 61). The tACS$_{site}$ was also included as an ROI, represented by a 10-mm sphere centered on the voxel with the maximal electric field (x, y, z = 16, −86, 36; Fig. 1A). More details are provided in *SI Appendix*, Table S1 and Fig. S2.

RS Functional Connectivity. Pre- and poststimulation fMRI timeseries from each of the six ROIs were submitted to Pearson's correlation analysis to construct a 5 × 5 correlation matrix for each session for each participant. The pairwise correlation coefficients were Fisher Z transformed before submission to statistical analyses. Seed-based whole-brain connectivity, with PCC and tACS site as seeds, was further evaluated to ascertain the extent of connectivity changes.

Statistical Analysis. We first established the efficacy of tACS by examining changes in alpha power and P→F connectivity. We then conducted ROI-based connectivity analyses for fMRI RS functional connectivity. These effects of tACS were evaluated with simple contrasts (paired t tests of pre versus post sessions) in the Active group ($P < 0.05$). To control for time-related confounds, we also performed double contrasts of pre versus post between Active and Sham groups (Active − Sham$_{Post − Pre}$; $P < 0.05$). Given the multiple ROIs considered in the analyses, we applied FDR correction to the double contrasts across the ROIs. Seed-based whole-brain connectivity was corrected with small-volume correction (FDR $P < 0.05$) in SPM12. We also submitted DMN source-level alpha-frequency GC to the same simple and double contrasts. Finally, to link EEG and fMRI effects of tACS, we submitted them into Pearson

correlation analyses ($P < 0.05$). Significant EEG-fMRI correlations were followed by mediation analyses to elucidate the contribution of alpha enhancement to α-tACS effects on DMN connectivity. The PROCESS macro for the Statistical Package for the Social Sciences (SPSS) (62) was used to estimate 5,000 bias-corrected bootstrap samples, from which a 95% CI was created to test the indirect effect of α-tACS on DMN connectivity through alpha activity.

Data Availability. Group-level contrasts of fMRI connectivity and EEG power/connectivity have been deposited in Neurovault (https://neurovault.org/collections/11913/) and GitHub (https://github.com/LiLabFSU/Alpha-DMN-association).

1. M. E. Raichle, A. Z. Snyder, A default mode of brain function: A brief history of an evolving idea. *Neuroimage* **37**, 1083–1090, discussion 1097–1099 (2007).
2. M. Shanahan, Metastable chimera states in community-structured oscillator networks. *Chaos* **20**, 013108 (2010).
3. G. Deco, M. Corbetta, The dynamical balance of the brain at rest. *Neuroscientist* **17**, 107–123 (2011).
4. E. Tagliazucchi, F. von Wegner, A. Morzelewski, V. Brodbeck, H. Laufs, Dynamic BOLD functional connectivity in humans and its electrophysiological correlates. *Front. Hum. Neurosci.* **6**, 339 (2012).
5. P. J. Uhlhaas et al., Neural synchrony in cortical networks: History, concept and current status. *Front. Integr. Nuerosci.* **3**, 17 (2009).
6. G. Buzsáki, A. Draguhn, Neuronal oscillations in cortical networks. *Science* **304**, 1926–1929 (2004).
7. D. S. Margulies et al., Situating the default-mode network along a principal gradient of macroscale cortical organization. *Proc. Natl. Acad. Sci. U.S.A.* **113**, 12574–12579 (2016).
8. R. L. Buckner, L. M. DiNicola, The brain's default network: Updated anatomy, physiology and evolving insights. *Nat. Rev. Neurosci.* **20**, 593–608 (2019).
9. M. D. Greicius, G. Srivastava, A. L. Reiss, V. Menon, Default-mode network activity distinguishes Alzheimer's disease from healthy aging: Evidence from functional MRI. *Proc. Natl. Acad. Sci. U.S.A.* **101**, 4637–4642 (2004).
10. S. Whitfield-Gabrieli et al., Hyperactivity and hyperconnectivity of the default network in schizophrenia and in first-degree relatives of persons with schizophrenia. *Proc. Natl. Acad. Sci. U.S.A.* **106**, 1279–1284 (2009).
11. T. J. Akiki, C. L. Averill, C. G. Abdallah, A network-based neurobiological model of PTSD: Evidence from structural and functional neuroimaging studies. *Curr. Psychiatry Rep.* **19**, 81 (2017).
12. M. D. Greicius et al., Resting-state functional connectivity in major depression: Abnormally increased contributions from subgenual cingulate cortex and thalamus. *Biol. Psychiatry* **62**, 429–437 (2007).
13. S. Palva, J. M. Palva, New vistas for alpha-frequency band oscillations. *Trends Neurosci.* **30**, 150–158 (2007).
14. W. Klimesch, P. Sauseng, S. Hanslmayr, EEG alpha oscillations: The inhibition-timing hypothesis. *Brain Res. Brain Res. Rev.* **53**, 63–88 (2007).
15. W. Tang et al., Dynamic connectivity modulates local activity in the core regions of the default-mode network. *Proc. Natl. Acad. Sci. U.S.A.* **114**, 9713–9718 (2017).
16. J. Mo, Y. Liu, H. Huang, M. Ding, Coupling between visual alpha oscillations and default mode activity. *Neuroimage* **68**, 112–118 (2013).
17. G. G. Knyazev, J. Y. Slobodskoj-Plusnin, A. V. Bocharov, L. V. Pylkova, The default mode network and EEG α oscillations: An independent component analysis. *Brain Res.* **1402**, 67–79 (2011).
18. K. Jann et al., BOLD correlates of EEG alpha phase-locking and the fMRI default mode network. *Neuroimage* **45**, 903–916 (2009).
19. J. Samogin, Q. Liu, M. Marino, N. Wenderoth, D. Mantini, Shared and connection-specific intrinsic interactions in the default mode network. *Neuroimage* **200**, 474–481 (2019).
20. R. Scheeringa, K. M. Petersson, A. Kleinschmidt, O. Jensen, M. C. M. Bastiaansen, EEG α power modulation of fMRI resting-state connectivity. *Brain Connect.* **2**, 254–264 (2012).
21. A. Hillebrand et al., Direction of information flow in large-scale resting-state networks is frequency-dependent. *Proc. Natl. Acad. Sci. U.S.A.* **113**, 3867–3872 (2016).
22. A. Coito, C. M. Michel, S. Vulliemoz, G. Plomp, Directed functional connections underlying spontaneous brain activity. *Hum. Brain Mapp.* **40**, 879–888 (2019).
23. J. J. Foxe, A. C. Snyder, The role of alpha-band oscillations as a sensory suppression mechanism during selective attention. *Front. Psychol.* **2**, 154 (2011).
24. Z. Jafari, B. E. Kolb, M. H. Mohajerani, Neural oscillations and brain stimulation in Alzheimer's disease. *Prog. Neurobiol.* **194**, 101878 (2020).
25. M. M. A. Engels et al., Directional information flow in patients with Alzheimer's disease. A source-space resting-state MEG study. *Neuroimage Clin.* **15**, 673–681 (2017).
26. K. J. Clancy et al., Posttraumatic stress disorder is associated with α dysrhythmia across the visual cortex and the default mode network. *eNeuro* **7**, ENEURO.0053-20.2020 (2020).
27. A. Vossen, J. Gross, G. Thut, Alpha power increase after transcranial alternating current stimulation at alpha frequency (α-tACS) reflects plastic changes rather than entrainment. *Brain Stimul.* **8**, 499–508 (2015).
28. K. J. Clancy et al., Lasting connectivity increase and anxiety reduction via transcranial alternating current stimulation. *Soc. Cogn. Affect. Neurosci.* **13**, 1305–1316 (2018).
29. F. H. Kasten, J. Dowsett, C. S. Herrmann, Sustained aftereffect of α-tACS lasts up to 70 min after stimulation. *Front. Hum. Neurosci.* **10**, 245 (2016).
30. S. Ahn et al., Targeting reduced neural oscillations in patients with schizophrenia by transcranial alternating current stimulation. *Neuroimage* **186**, 126–136 (2019).
31. P. Fries, A mechanism for cognitive dynamics: Neuronal communication through neuronal coherence. *Trends Cogn. Sci.* **9**, 474–480 (2005).
32. A. C. Tang et al., "Top-down versus bottom-up processing in the human brain: Distinct directional influences revealed by integrating SOBI and granger causality" in *Proceedings of the 7th International Conference on Independent Component Analysis and Signal Separation*, M. E. Davies, C. J. James, S. A. Abdallah, M. D. Plumbley, Eds. (Springer Berlin Heidelberg, Berlin, Heidelberg, London, UK, 9–12 September 2007), pp. 802–809. 10.1007/978-3-540-74494-8_100.
33. R. Wang et al., Consistency and dynamical changes of directional information flow in different brain states: A comparison of working memory and resting-state using EEG. *Neuroimage* **203**, 116188 (2019).
34. H. Zhang, A. J. Watrous, A. Patel, J. Jacobs, Theta and alpha oscillations are traveling waves in the human neocortex. *Neuron* **98**, 1269–1281.e1264 (2018).
35. M. S. Clayton, N. Yeung, R. Cohen Kadosh, The many characters of visual alpha oscillations. *Eur. J. Neurosci.* **48**, 2498–2508 (2018).
36. E. L. Johnson et al., Bidirectional frontoparietal oscillatory systems support working memory. *Curr. Biol.* **27**, 1829–1835.e1824 (2017).
37. C. S. Herrmann, S. Rach, T. Neuling, D. Strüber, Transcranial alternating current stimulation: A review of the underlying mechanisms and modulation of cognitive processes. *Front. Hum. Neurosci.* **7**, 279 (2013).
38. D. Reato, A. Rahman, M. Bikson, L. C. Parra, Effects of weak transcranial alternating current stimulation on brain activity—A review of known mechanisms from animal studies. *Front. Hum. Neurosci.* **7**, 687 (2013).
39. M. Bächinger et al., Concurrent tACS-fMRI reveals causal influence of power synchronized neural activity on resting state fMRI connectivity. *J. Neurosci.* **37**, 4766–4777 (2017).
40. Y. Cabral-Calderin, K. A. Williams, A. Opitz, P. Dechent, M. Wilke, Transcranial alternating current stimulation modulates spontaneous low frequency fluctuations as measured with fMRI. *Neuroimage* **141**, 88–107 (2016).
41. K. Kar, T. Ito, M. W. Cole, B. Krekelberg, Transcranial alternating current stimulation attenuates BOLD adaptation and increases functional connectivity. *J. Neurophysiol.* **123**, 428–438 (2020).
42. A. Bollimunta, J. Mo, C. E. Schroeder, M. Ding, Neuronal mechanisms and attentional modulation of corticothalamic α oscillations. *J. Neurosci.* **31**, 4935–4943 (2011).
43. R. Rajagovindan, M. Ding, From prestimulus alpha oscillation to visual-evoked response: An inverted-U function and its attentional modulation. *J. Cogn. Neurosci.* **23**, 1379–1394 (2011).
44. B. D. Hare, R. S. Duman, Prefrontal cortex circuits in depression and anxiety: Contribution of discrete neuronal populations and target regions. *Mol. Psychiatry* **25**, 2742–2758 (2020).
45. R. M. Braga, K. R. A. Van Dijk, J. R. Polimeni, M. C. Eldaief, R. L. Buckner, Parallel distributed networks resolved at high resolution reveal close juxtaposition of distinct regions. *J. Neurophysiol.* **121**, 1513–1534 (2019).
46. R. Leech, S. Kamourieh, C. F. Beckmann, D. J. Sharp, Fractionating the default mode network: Distinct contributions of the ventral and dorsal posterior cingulate cortex to cognitive control. *J. Neurosci.* **31**, 3217–3224 (2011).
47. M. M. Halassa, S. M. Sherman, Thalamocortical circuit motifs: A general framework. *Neuron* **103**, 762–770 (2019).
48. V. Crunelli, F. David, M. L. Lőrincz, S. W. Hughes, The thalamocortical network as a single slow wave-generating unit. *Curr. Opin. Neurobiol.* **31**, 72–80 (2015).
49. G. Buzsáki, N. Logothetis, W. Singer, Scaling brain size, keeping timing: Evolutionary preservation of brain rhythms. *Neuron* **80**, 751–764 (2013).
50. R. R. Llinás, U. Ribary, D. Jeanmonod, E. Kronberg, P. P. Mitra, Thalamocortical dysrhythmia: A neurological and neuropsychiatric syndrome characterized by magnetoencephalography. *Proc. Natl. Acad. Sci. U.S.A.* **96**, 15222–15227 (1999).
51. P.-C. Tu et al., Identification of common thalamocortical dysconnectivity in four major psychiatric disorders. *Schizophr. Bull.* **45**, 1143–1151 (2019).
52. J. D. Power, K. A. Barnes, A. Z. Snyder, B. L. Schlaggar, S. E. Petersen, Spurious but systematic correlations in functional connectivity MRI networks arise from subject motion. *Neuroimage* **59**, 2142–2154 (2012).
53. S. Alagapan et al., Modulation of cortical oscillations by low-frequency direct cortical stimulation is state-dependent. *PLoS Biol.* **14**, e1002424 (2016).
54. A. R. Brunoni et al., A systematic review on reporting and assessment of adverse effects associated with transcranial direct current stimulation. *Int. J. Neuropsychopharmacol.* **14**, 1133–1145 (2011).

NEUROSCIENCE

PSYCHOLOGICAL AND COGNITIVE SCIENCES

Clancy et al.
Transcranial stimulation of alpha oscillations up-regulates the default mode network

PNAS | 7 of 8
https://doi.org/10.1073/pnas.2110868119

55. FIL Methods Group, SPM12. https://www.fil.ion.ucl.ac.uk/spm/software/spm12. Accessed 22 December 2021.

56. R. D. Pascual-Marqui *et al.*, Assessing interactions in the brain with exact low-resolution electromagnetic tomography. *Philos. Trans.- Royal Soc., Math. Phys. Eng. Sci.* **369**, 3768–3784 (2011).

57. J. Xu *et al.*, Evaluation of slice accelerations using multiband echo planar imaging at 3 T. *Neuroimage* **83**, 991–1001 (2013).

58. B. T. Yeo *et al.*, The organization of the human cerebral cortex estimated by intrinsic functional connectivity. *J. Neurophysiol.* **106**, 1125–1165 (2011).

59. A. Altmann, B. Ng, S. M. Landau, W. J. Jagust, M. D. Greicius; Alzheimer's Disease Neuroimaging Initiative, Regional brain hypometabolism is unrelated to regional amyloid plaque burden. *Brain* **138**, 3734–3746 (2015).

60. L. Fan *et al.*, The human brainnetome atlas: A new brain atlas based on connectional architecture. *Cereb. Cortex* **26**, 3508–3526 (2016).

61. J. R. Andrews-Hanna, J. S. Reidler, J. Sepulcre, R. Poulin, R. L. Buckner, Functional-anatomic fractionation of the brain's default network. *Neuron* **65**, 550–562 (2010).

62. A. F. Hayes, *Introduction to Mediation, Moderation, and Conditional Process Analysis: A Regression-Based Approach* (Guilford Press, New York, NY, 2013), pp. xvii, 507.

63. K. Clancy, M. Ding, E. Bernat, N. B. Schmidt, W. Li, Restless 'rest': Intrinsic sensory hyperactivity and disinhibition in post-traumatic stress disorder. *Brain* **140**, 2041–2050 (2017).

64. K. J. Clancy, A. Albizu, N. B. Schmidt, W. Li, Intrinsic sensory disinhibition contributes to intrusive re-experiencing in combat veterans. *Sci. Rep.* **10**, 936 (2020).